# Modulation of Ligand Fluorescence by the Pt(II)/Pt(IV) Redox Couple

Justin J. Wilson, Stephen J. Lippard *

*Department of Chemistry, Massachusetts Institute of Technology, Cambridge, MA 02139, United States*

* Corresponding Author.
*Email Address*: lippard@mit.edu (S.J. Lippard)

**Abstract**
The dangling carboxylic acid moiety of the known platinum(II) complex, [Pt(edma)$Cl_2$] (edma = ethylenediaminemonoacetic acid), was functionalized via amide coupling chemistry with benzyl amine and dansyl ethylenediamine to afford the derivatives [Pt(edBz)$Cl_2$] (**1**) and [Pt(edDs)$Cl_2$] (**2**). Subsequent oxidation of these platinum(II) complexes with iodobenzene dichloride in DMF yielded the respective platinum(IV) analogues, [Pt(edBz)$Cl_4$] (**3**) and [Pt(edDs)$Cl_4$] (**4**). All four platinum complexes were characterized by multinuclear NMR spectroscopy, IR spectroscopy, electrospray ionization mass spectrometry, and elemental analysis. In addition, compounds **1** and **3** were structurally characterized by X-ray crystallography. The photophysical properties of the compounds bearing the fluorescent dansyl moiety, **2** and **4**, were evaluated. The emission quantum yields of **2** and **4** in DMF are 27% and 1.6%, respectively. This large difference in emission efficiency indicates that the platinum(IV) center in **4** is more effective at quenching the dansyl-based fluorescence than the platinum(II) center in **2**. Time-dependent density functional theory calculations indicate that **4** has several low-lying singlet excited states that energetically lie below the primary radiation-accessible excited state of the dansyl fluorophore. These low-energy excited states may offer non-radiative decay pathways that lower the overall emission quantum yield. Treatment of **4** with biologically relevant reducing agents in pH 7.4 phosphate-buffered saline induces a 6.3-fold increase in emission intensity. These results demonstrate that **4** and future derivatives thereof may be useful for imaging the reduction of platinum(IV) complexes in living systems, chemistry of importance for future platinum-based anticancer drug strategies.

**Keywords**
platinum(IV) anticancer agents; fluorescence; dansyl; cisplatin; DFT calculations; X-ray structures

**Dedication**
Dedicated to Professor Jon Zubieta on the occasion of his 65$^{th}$ birthday.

## 1. Introduction

Platinum-based drugs are effective agents for a number of different cancers [1, 2]. Dose-limiting toxic side effects and acquired resistance, however, limit the broader applicability of this class of compounds. The search for new platinum anticancer agents with fewer such drawbacks is an active area of research [3, 4]. Among the new classes of platinum compounds explored, octahedral platinum complexes in the +4 oxidation state show considerable promise. Platinum(IV) anticancer complexes have several advantages over first- and second-generation square-planar platinum(II) analogues [5-7]. The additional two ligand-binding sites enable synthetic modification and fine tuning of the pharmacokinetic parameters. Compared to platinum(II) complexes, however, the mechanism of action of platinum(IV) complexes is less well understood. In most cases, these complexes are best reduced first by two electrons to form square-planar platinum(II) complexes in a process that facilitates binding to proteins, DNA, or other cellular targets [8]. Still, questions remain about this reductive activation step. It is not clear as to how quickly, by what means, and where such reduction occurs in living systems. X-ray fluorescence and absorption spectroscopy [9-11] has been used to address these questions. These methodologies, however, are not applicable to live cells and generally require synchrotron radiation.

Optical fluorescence microscopy for imaging analytes and processes in living systems is well established [12]. This method has been used to study the cellular localization and uptake of platinum-fluorophore conjugates, which were designed as models for related platinum anticancer drugs [13-15]. Although fluorescence microscopy, unlike X-ray techniques, cannot directly provide information about the oxidation state of metal ions, it is possible to apply ligand systems in which the fluorescence intensity is modulated depending on the oxidation state of the

coordinated metal [16, 17]. Such a system involving the Pt(IV)/Pt(II) redox couple has recently been described [18], in which analogous platinum(II) and platinum(IV) complexes were coordinated to fluorescent coumarin ligands by means of an aniline functional group on the dye. The authors reported a 7-fold greater emission intensity for the platinum(II) compared to the platinum(IV) complex in DMF solution. Furthermore, confocal fluorescence microscopic imaging analyses revealed strong localization of the complexes in the cytosol and lysosomes. The free coumarin ligands exhibited cellular localization similar to that of the complexes, thus raising the possibility that the coumarin ligands are displaced from platinum in the cell. Similar systems with strongly coordinated bidentate ligands may be able to provide information about platinum(IV) reduction in live cells.

In the present article we describe our work to design a platinum-fluorophore conjugate that can be used to monitor platinum(IV) reduction in living systems by an emissive turn-on response. We present the synthesis and characterization of the dansyl fluorophore-bearing platinum(II) and platinum(IV) complexes, **2** and **4**, as well as non-fluorescent analogues **1** and **3** (Scheme 1). Photophysical studies of **2** and **4** indicate the platinum(IV) complex to have a significantly lower emission quantum yield than the platinum(II) complex; upon reduction of **4**, a 6.3-fold emission turn-on response is observed in aqueous buffer. Additionally, computational studies are reported that rationalize the increased fluorescence quenching of **4**.

**Scheme 1**

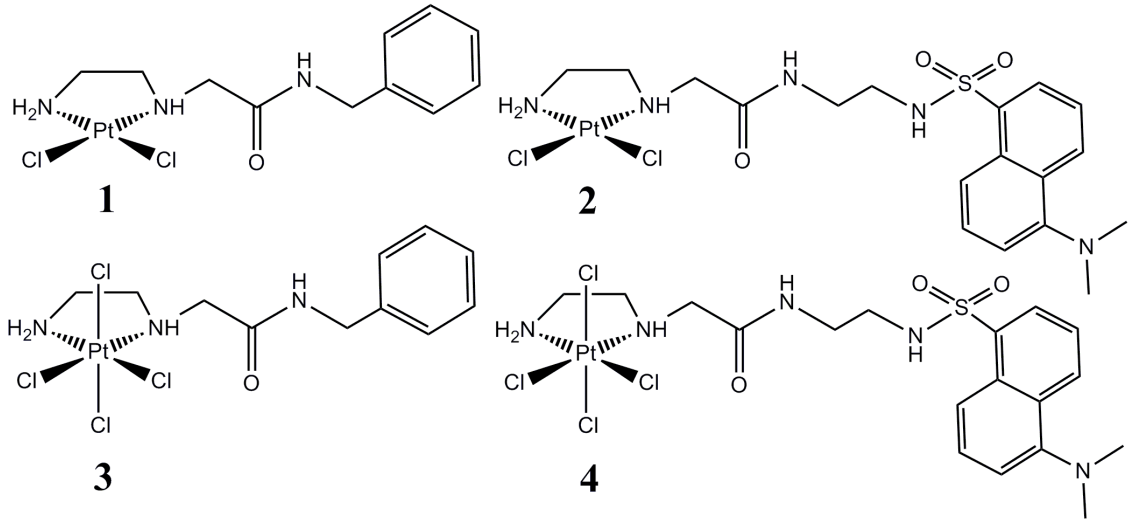


## 2. Experimental Section

### *2.1. General Considerations*

All reactions were carried out under normal atmospheric conditions. Solvents were used as received without additional drying or purification. The compounds, [Pt(edma)$Cl_2$] (edma = ethylenediaminemonoacetic acid) [19], dansyl ethylenediamine (Ds-en) [20], and iodobenzene dichloride [21], were synthesized as previously described. Benzylamine and carbonyldiimidazole (CDI) were purchased from Sigma Aldrich and used as received.

### *2.2. Physical Measurements*

NMR spectra were recorded on a Bruker DPX-400 spectrometer in the MIT Department of Chemistry Instrumentation Facility at 20 °C. $^{1}H$ and $^{13}C\{^{1}H\}$ NMR spectra were referenced internally to residual solvent peaks, and chemical shifts are expressed relative to tetramethylsilane, $SiMe_4$ ($\delta = 0$ ppm). $^{195}Pt\{^{1}H\}$ NMR spectra were referenced externally to $K_2PtCl_4$ in $D_2O$ ($\delta = -1628$ ppm). NMR spectra of all compounds are shown in the Supplementary Data (Figs. S1–S22). Fourier transform infrared (FTIR) spectra were recorded

with a ThermoNicolet Avatar 360 spectrometer running the OMNIC software. Samples were prepared as KBr disks. Cyclic voltammograms were obtained at room temperature using a VersaSTAT3 potentiostat from Princeton Applied Research accompanied by the V3 Studio software. A three-electrode system was used, comprising a glassy carbon working electrode, a Pt wire auxiliary electrode, and a Ag/AgCl (aqueous saturated NaCl) reference electrode. Samples were prepared as 2 mM solutions in DMF with 0.1 M $(Bu_4N)(PF_6)$ as the supporting electrolyte. Peak potentials are reported at a scan rate of 100 mV/s. The ferrocene/ferrocenium redox couple was 0.54 – 0.55 V vs Ag/AgCl using the setup described here. Optical absorption spectra were recorded with a Cary 1E spectrophotometer. Emission spectra were obtained with a Photon Technology International QM-4/2003 fluorimeter. Quantum yields for fluorescence were measured using quinine sulfate in 0.1 M $H_2SO_4$ ($\Phi = 0.58$) as the reference [22] over a range of at least five different absorbance values. For measuring these values in phosphate buffered saline (PBS), the samples were diluted from DMF solutions to give aqueous solutions containing less than or equal to 1% DMF. For all photophysical measurements, the sample temperature was maintained at 25.0 ± 0.5 °C using a circulating water bath.

*2.3. Synthesis of [Pt(edBz)Cl$_2$] (**1**)*

A solution of CDI (0.230 g, 1.42 mmol) in 10 mL of DMF was added to a solution of $[Pt(edma)Cl_2]$ (0.535 g, 1.39 mmol) in 10 mL of DMF. The resulting mixture was heated at 60 °C for 10 min, and then sparged with $N_2$ for 5 min. Benzylamine (0.152 g, 1.42 mmol) in 15 mL of DMF was added dropwise to the solution containing the activated platinum complex. After stirring for 12 h, the solution was concentrated to 10 mL under reduced pressure and elevated temperature (60 °C) and then filtered through Celite. The addition of 10 mL of water afforded the desired compound as a pale yellow solid, which was isolated by filtration and washed

sequentially with 5 mL of water, 2 × 5 mL of ethanol, and 2 × 5 mL of diethyl ether before being dried in vacuo. Yield: 0.268 g (40%). M.p. 298–300 °C (dec). $^{1}$H NMR (400 MHz, DMF-$d_7$): δ 8.60 (t, 1H), 7.35 – 7.26 (m, 5H), 6.15 (br s, 1H), 5.48 (br s, 2H), 4.43 (d, 2H), 4.27 (d, 1H), 3.71 (dd, 1H), 3.12 – 3.07 (br m, 1H), 2.82 – 2.72 (br m, 2H), 2.57 – 2.55 (br m, 1H). $^{13}$C{$^{1}$H} NMR (100 MHz, DMF-$d_7$): δ 168.2, 139.4, 128.6, 127.7, 127.2, 57.8, 55.1, 47.3, 42.8. $^{195}$Pt{$^{1}$H} NMR (86 MHz, DMF-$d_7$): δ -2339. IR (KBr, cm$^{-1}$): 3335 m, 3274 s, 3202 m, 2940 w, 1654 vs, 1576 m, 1545 s, 1455 w, 1436 m, 1425 m, 1392 vw, 1279 w, 1243 m, 1168 w, 1116 w, 1091 w, 1041 w, 967 w, 758 m, 702 s, 611 w, 572 w, 525 w. ESI-MS (negative-ion mode): *m/z* 509.4 [M+Cl]$^-$, 944.6 [2M–H]$^-$, 980.9 [2M+Cl]$^-$. Anal. Calcd. for $C_{11}H_{17}Cl_2N_3OPt$: C, 27.92; H, 3.62; N, 8.88. Found: C, 28.30; H, 3.65; N, 8.85.

*2.4. Synthesis of [Pt(edDs)Cl$_2$] (**2**)*

A solution of CDI (0.206 g, 1.27 mmol) in 20 mL of DMF was added to a solution of [Pt(edma)Cl$_2$] (0.469 g, 1.21 mmol) in 16 mL of DMF, and the resulting mixture was stirred at 60 °C for 10 min. The solution was sparged with $N_2$ for 5 min, and then Ds-en (0.372 g, 1.27 mmol) in 20 mL of DMF was added dropwise. After stirring at r.t. for 12 h, the mixture was concentrated to 10 mL under vacuum and increased temperature (60 °C), and then filtered through Celite. Water (10 mL) was added to the filtrate to precipitate the desired compound. The pale yellow solid was isolated by filtration, and washed sequentially with water, ethanol, and diethyl ether. Yield: 0.471 g (59%). M.p. 258–262 °C (dec). $^{1}$H NMR (400 MHz, DMF-$d_7$): δ 8.55 (d, 1H), 8.39 (d, 1H), 8.28 (t, 1H), 8.20 (d, 1H), 7.97 (br t, 1H), 7.68 (t, 1H), 7.62 (t, 1H), 7.30 (d, 1H), 6.03 (br s, 1H), 5.44 (br s, 2H), 4.12 (d, 1H), 3.49 – 3.45 (m, 1H), 3.29 – 3.26 (m, 2H), 3,01 – 2.96 (m, 3H), 2.88 (s, 6H), 2.69 (br m, 2H), 2.44 (br m, 1H). $^{13}$C{$^{1}$H} NMR (100 MHz, DMF-$d_7$): δ 168.4, 152.2, 136.6, 130.01, 129.99, 129.8, 128.9, 128.2, 123.9, 119.7, 115.6,

57.7, 55.1, 47.3, 45.2, 42.5, 39.6. $^{195}$Pt{$^{1}$H} NMR (86 MHz, DMF-$d_7$): δ -2345. IR (KBr, cm$^{-1}$): 3351 m, 3270 m, 3192 m, 3141 m, 2946 w, 1659 vs, 1571 w, 1547 w, 1318 s, 1144 s, 1095 w, 788 s, 629 w, 576 w. ESI-MS (negative-ion mode): *m/z* 657.8 [M–H]$^-$. Anal. Calcd. for $C_{18}H_{27}Cl_2N_5O_3PtS$: C, 32.78; H, 4.13; N, 10.62. Found: C, 32.92; H, 4.12; N, 10.77.

*2.5. Synthesis of [Pt(edBz)Cl$_4$] (**3**)*

[Pt(edBz)Cl$_2$] (0.120 g, 0.250 mmol) was dissolved in 10 mL of DMF with gentle heating at 60 °C. To this solution, iodobenzene dichloride (0.072 g, 0.26 mmol) in 1 mL of DMF was added dropwise. The solution changed color immediately from pale yellow to bright yellow. After stirring 3 h at r.t., a 25 mL portion of diethyl ether was added, and the resulting bright yellow solid was collected by filtration. It was further washed with diethyl ether and then dried in vacuo. Yield: 0.086 g (63%). M.p. 188–198 °C (dec). $^{1}$H NMR (400 MHz, DMF-$d_7$): δ 8.90 (t, 1H), 7.92 (br s, unresolved $^{195}$Pt satellites, 1H), 7.68 (br s, unresolved $^{195}$Pt satellites, 1H), 7.39–7.27 (m, 5H), 7.10 (br s, $^{2}J_{PtH}$ = 56 Hz, 1H), 4.51–4.43 (m, 3H), 3.93–3.83 (m, 1H), 3.36–3.20 (br m, 3H), 2.88 (br m, 1H). $^{13}$C{$^{1}$H} NMR (100 MHz, DMF-$d_7$): δ 166.7, 139.2, 128.7, 127.8, 127.4, 59.2, 54.5, 47.8, 43.2. $^{195}$Pt{$^{1}$H} NMR (86 MHz, DMF-$d_7$): δ -382. IR (KBr, cm$^{-1}$): 3224 m, 3075 m, 3027 m, 2961 w, 1656 vs, 1571 m, 1496 vw, 1453 w, 1409 w, 1329 w, 1298 w, 1266 w, 1203 vw, 1131 vw, 1098 w, 1048 w, 750 m, 701 m, 662 w, 613 w, 595 w, 575 w. ESI-MS (negative-ion mode): *m/z* 542.5 [M–H]$^-$, 1086.6 [2M–H]$^-$. Anal. Calcd. for $C_{11}H_{17}Cl_4N_3OPt$: C, 24.28; H, 3.15; N, 7.72. Found: C, 24.66; H, 3.36; N, 7.43.

*2.6. Synthesis of [Pt(edDs)Cl$_4$] (**4**)*

A solution of iodobenzene dichloride (0.107 g, 0.390 mmol) in 2 mL of DMF was added dropwise to a solution of [Pt(edDs)Cl$_2$] (0.250 g, 0.379 mmol) in 16 mL of DMF. The color of the solution changed immediately from pale yellow to pale orange. After stirring 12 h at r.t., 80

mL of diethyl ether was added to form a sticky residue on the flask bottom. The diethyl ether and DMF were decanted, and 30 mL of water was added to the residue. The resulting solid was collected by filtration. It was suspended sequentially in water, methanol, and diethyl ether before being dried in vacuo. Yield: 0.103 g (33%). M.p. 245–254 °C (dec). $^{1}$H NMR (400 MHz, DMSO-$d_6$): δ 8.57–8.53 (m, 2H), 8.41 (d, 1H), 8.23 (d, 1H), 8.01 (t, 1H), 7.90 (br s, 1H), 7.71–7.61 (m, 3H), 7.32 (d, 1H), 6.92 (br s, $^{2}J_{PtH}$ = 58 Hz, 1H), 4.35–4.30 (m, 1H), 3.74–3.68 (m, 1H), 3.37–3.29 (m, 3H), 3.16–3.05 (m, 5H), 2.89 (s, 6H). $^{13}$C{$^{1}$H} NMR (100 MHz, DMF-$d_7$): δ 166.7, 152.0, 136.6, 130.0, 129.9, 129.8, 128.9, 128.2, 123.9, 119.8, 115.6, 58.9, 54.3, 47.7, 45.2, 42.3, 40.0. $^{195}$Pt{$^{1}$H} NMR (86 MHz, DMF-$d_7$): δ -386. IR (KBr, cm$^{-1}$): 3346 s, 3307 m, 3185 m, 3075 m, 2956 w, 2872 w, 2790 w, 1688 vs, 1613 w, 1573 m, 1543 m, 1480 w, 1450 m, 1431 m, 1412 m, 1316 s, 1254 w, 1234 w, 1158 s, 1141 vs, 1085 m, 1063 m, 1041 m, 960 m, 942 m, 910 w, 839 w, 814 m, 788 s, 681 w, 627 s, 574 s, 554 w, 499 w. ESI-MS (negative-ion mode): *m/z* 728.5 [M–H]$^{-}$, 1458.6 [2M–H]$^{-}$. Anal. Calcd. for $C_{18}H_{27}Cl_4N_5O_3PtS$: C, 29.60; H, 3.73; N, 9.59. Found: C, 29.55; H, 3.71; N, 9.36.

*2.7. Theoretical Calculations*

Density functional theory (DFT) calculations were performed with the Gaussian 03 (Rev.D01) software package [23]. All calculations were carried out using the B3LYP functional [24, 25]. The LANL2DZ basis set and effective core potential [26] was used for the Pt atom and the 6-31++G(d,p) basis set [27] was used for all other atoms. Geometries of **2** and **4** were optimized in the gas phase and established as local minima by frequency calculations, which revealed no imaginary values. The conductor-like polarizable continuum model (CPCM) [28] was applied for subsequent molecular orbital and time-dependent DFT (TDDFT) calculations to simulate solvation of the compounds in water. The TDDFT calculations were used to determine

the natures, energies, and oscillator strengths of the 50 lowest energy singlet excited states. Relevant Kohn-Sham molecular orbitals, the XYZ-coordinates of optimized structures, and a summary the lowest energy (< 4.09 eV, > 303 nm) singlet excited states are provided in the Supplementary Data (Figs. S23 and S24, Tables S1–S4).

*2.8. X-ray Crystallographic Studies*

Single crystals of **1**·DMF and **3**·DMF were grown by vapor diffusion of diethyl ether into DMF solutions. The single crystals were mounted in Paratone oil on a cryoloop and frozen under a 100 K KRYO-FLEX nitrogen cold stream. Data were collected on a Bruker APEX CCD X-ray diffractometer with graphite-monochromated Mo-Kα radiation (λ = 0.71073 Å) controlled by the *APEX2* software package [29]. Absorption corrections were applied using *SADABS* [30]. The structures were solved using direct methods and refined on $F^2$ with the *SHELXTL-97* software package [31, 32]. Structures were checked for higher symmetry using *PLATON* [33]. All non-hydrogen atoms were located and refined anisotropically. Hydrogen atoms were placed in idealized locations and given isotropic thermal parameters equivalent to either 1.5 (terminal $CH_3$ or $NH_3$ hydrogen atoms) or 1.2 times the thermal parameter of the atom to which they were attached. The highest residual electron density peaks and holes after complete refinement were located less than 1.33 Å from the platinum atom in the structures of both **1** and **3**. Crystallographic data collection and refinement parameters are shown in Table 1.

**Table 1.** X-ray Crystallographic Data Collection and Refinement Parameters.

| | **1**·DMF | **3**·DMF |
|---|---|---|
| formula | $C_{14}H_{24}Cl_2N_4O_2Pt$ | $C_{14}H_{24}Cl_4N_4O_2Pt$ |
| fw | 546.36 | 617.26 |
| space group | $P2_1/c$ | $P2_1/c$ |
| *a*, Å | 13.7730(9) | 14.4637(8) |
| *b*, Å | 12.6440(8) | 11.2251(6) |
| *c*, Å | 11.2843(7) | 13.3621(8) |
| β, deg | 102.6200(10) | 109.8980(10) |
| *V*, Å $^3$ | 1917.6(2) | 2039.9(2) |
| *Z* | 4 | 4 |
| $\rho_{calcd}$, g·cm$^{-3}$ | 1.892 | 2.010 |
| *T*, °C | -173(2) | -173(2) |
| μ(Mo Kα), mm$^{-1}$ | 7.608 | 7.418 |
| θ range, deg | 1.52–29.61 | 1.50–25.05 |
| total no. of data | 41701 | 31699 |
| no. of unique data | 5382 | 3604 |
| no. of parameters | 210 | 228 |
| completeness to θ (%) | 99.8 | 99.8 |
| R1[a] (%) | 2.49 | 3.42 |
| wR2[b] (%) | 3.95 | 6.98 |
| GOF[c] | 1.074 | 1.086 |
| max, min peaks, eÅ$^{-3}$ | 1.123, -0.447 | 2.011, -0.894 |

[a] $R1 = \Sigma||F_o| - |F_c||/\Sigma|F_o|$. [b] $wR2 = \{\Sigma[w(F_o^2 - F_c^2)^2]/\Sigma[w(F_o^2)^2]\}^{1/2}$. [c] $GOF = \{\Sigma[w(F_o^2 - F_c^2)^2]/(n-p)\}^{1/2}$ where *n* is the number of data and *p* is the number of refined parameters.

## 3. Results and Discussion

### *3.1. Synthesis and Characterization*

The platinum(II) complexes, **1** and **2**, were prepared by an amide coupling reaction between [Pt(edma)$Cl_2$] and benzylamine or Ds-en, respectively (Scheme 2). This amide

coupling reaction can be used to tether other desired amines to the core platinum(II) moiety. It is analogous to the amide coupling chemistry that has been employed to conjugate chemical moieties to the platinum(IV) complex, *cct*-[$Pt(NH_3)_2Cl_2(O_2CC_2H_4CO_2H)_2$], a derivative of cisplatin [34, 35]. Similar platinum(II) and platinum(IV) complexes bearing ethylenediamine-N,N'-diester ligands have been reported previously [36]. In these cases, however, the esterified ligands were prepared prior to metallation. For a series of platinum(II) peptide conjugates that were synthesized on a solid-phase support, it was necessary to protect the platinum-chelating unit during the synthesis of the peptide fragment [37, 38]. The advantage of performing the coupling reaction directly on the coordinated ligand, as demonstrated here, is that it eliminates the need for protecting groups during organic or peptide synthesis. We envision that this synthetic approach will be general and provide access to a range of interesting functionalized platinum(II) complexes.

**Scheme 2**

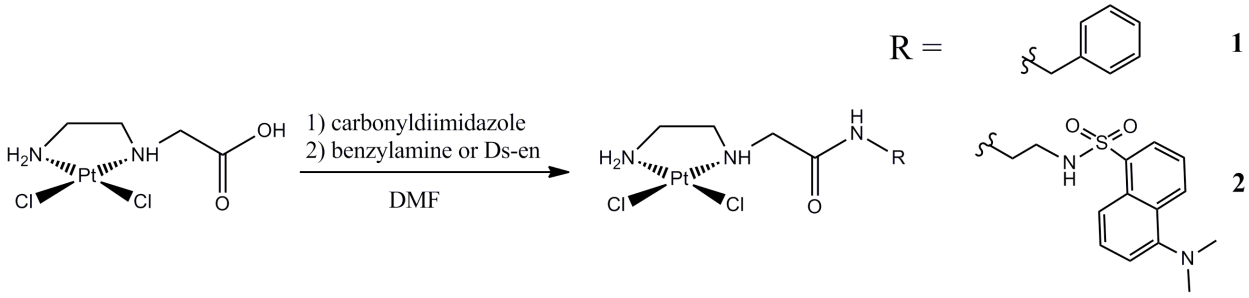


Clean oxidation of **1** and **2** to their Pt(IV) derivatives was accomplished with the hypervalent iodine reagent, iodobenzene dichloride (Scheme 3). By multinuclear NMR spectroscopy, we determined that only the tetrachloroplatinum(IV) complexes **3** and **4** were formed. The use of hydrogen peroxide as the oxidant in either water or acetic acid gave rise to a mixture of at least three different platinum(IV) compounds, as revealed by $^{195}Pt$ NMR

spectroscopy. Alternative hypervalent iodine reagents, $PhI(OAc)_2$, PhI(OH)(OTs), and 2,6-dimethyliodosylbenzene, failed to oxidize **1** and **2** under similar conditions.

**Scheme 3**

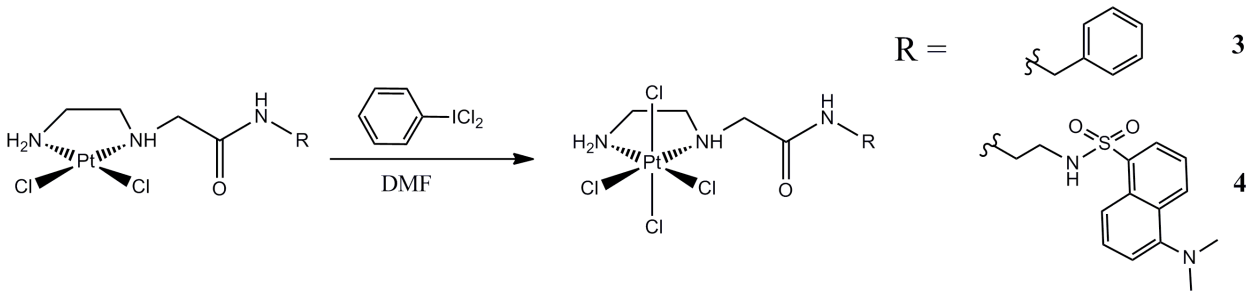


Characterization of the platinum complexes was carried out by conventional spectroscopic methods. The starting material for **1** and **2**, [Pt(edma)$Cl_2$], has a strong absorption in its IR spectrum at 1720 $cm^{-1}$, which is assigned to the C=O stretching frequency of the carboxylic acid. In **1** and **2**, this absorption is replaced by lower energy C=O vibrations at 1654 and 1659 $cm^{-1}$, respectively, consistent with the disappearance of the free carboxylic acid and formation of an amide bond. In the IR spectra of **3** and **4**, these absorptions occur at 1656 and 1688 $cm^{-1}$, respectively. The presence of the dansyl fluorophore in **2** and **4** was verified by the presence of S=O stretching frequencies from the sulfone moiety. The asymmetric and symmetric S=O stretches of **2** occur at 1318 and 1144 $cm^{-1}$, and those of **4** are at 1316 and 1141 $cm^{-1}$.

The $^{1}H$ and $^{13}C$ NMR spectra of **1** – **4** are consistent with the proposed structures. Peak assignments were made using 2-D COSY and $^{1}H$,$^{13}C$-HSQC NMR techniques as detailed in the Supplementary Data (Figs. S1 – S22). The aliphatic regions of the $^{1}H$ NMR spectra are characterized by complex splitting patterns due diastereotopic protons on and near the ethylenediamine backbone. Upon formation of the platinum(IV) complexes, resonances due to the coordinated NH and $NH_2$ groups shift downfield, consistent with oxidation of the platinum

center (Figure 1). Additionally, the NH resonances of the coordinated secondary amine in the platinum(IV) complexes display satellites arising from coupling to the $^{195}$Pt nucleus ($I$=1/2, 33%), with $^{2}J_{PtH}$ = 56 and 58 Hz for **3** and **4**, respectively. Platinum(IV) complexes give rise to well-resolved Pt satellites, unlike those of platinum(II) [39]. The $^{13}$C NMR spectra display all anticipated resonances. The $^{195}$Pt NMR spectra of **1** and **2** reveal resonances at -2339 and -2345 ppm, respectively. These values are typical for platinum(II) in an $N_2Cl_2$ coordination environment [40, 41], and the similarity between them indicates that the peripheral substituents on the amide do not significantly affect shielding at the platinum nucleus. The $^{195}$Pt chemical shifts of **3** and **4** are -382 and -386 ppm. These large downfield shifts relative to those of **1** and **2** are consistent with oxidation to platinum(IV). As with **1** and **2**, their close proximity indicates that the electronic environments of the platinum centers are substantially the same.

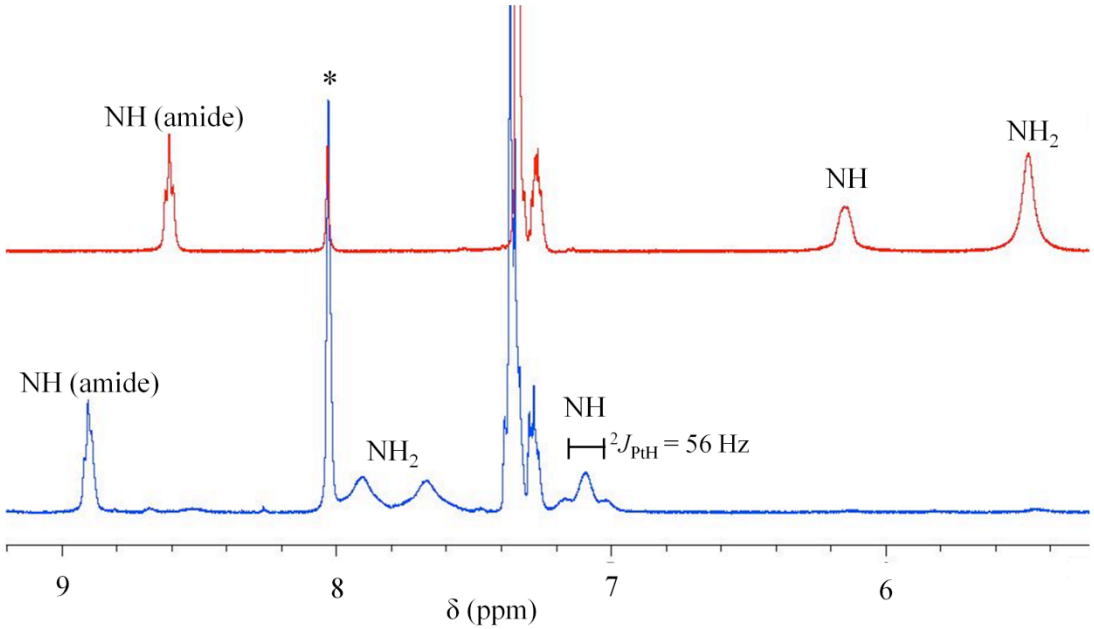


**Fig. 1.** Aromatic region of the $^{1}$H NMR spectra of **1** (top) and **3** (bottom) obtained at 20°C and 400 MHz in DMF-$d_7$. The asterisk marks the signal due to the solvent.

Single crystals of **1**·DMF and **3**·DMF were grown by diffusion of diethyl ether into DMF solutions of the complexes, and X-ray diffraction analyses revealed their structures, which are depicted in Figures 2 and 3. Relevant bond distances and angles for **1** are given in Table 2. The square-planar geometry and bond lengths are typical of Pt(II) complexes. A molecule of DMF is in the crystal lattice of **1** and forms a hydrogen bonding interaction with the NH group of the amide linkage, with $O_{DMF}\cdots N_{amide}$ = 2.83 Å. Also present in the lattice are short intermolecular Pt–Pt interactions (Figure 2, right), marked by a Pt–Pt distance of 3.30 Å. The X-ray crystal structure of the analogous compound, $[Pt(en)Cl_2]$ (en = ethylenediamine), has been determined for two distinct polymorphs [42, 43]. A careful crystal packing analysis of these polymorphs revealed close Pt–Pt intermolecular interactions, similar to those observed for **1**. In the orthorhombic form [42], the Pt–Pt separation is 3.38 Å, whereas the Pt–Pt separation in the triclinic polymorph [43] is 3.42 Å. These Pt–Pt interactions are supported by hydrogen bonds between the chloride ligands and coordinated amine protons of the neighboring molecules. The reason for the slightly shorter Pt–Pt distance in **1** compared to $[Pt(en)Cl_2]$ is not immediately obvious.

**Table 2.** Interatomic Distances (Å) and Angles (deg) for **1**.[a]

| Bonds | | Angles | |
|---|---|---|---|
| Pt(1)-N(1) | 2.024(2) | N(1)-Pt(1)-N(2) | 84.14(7) |
| Pt(1)-N(2) | 2.0425(18) | N(1)-Pt(1)-Cl(1) | 90.87(5) |
| Pt(1)-Cl(1) | 2.3142(5) | N(1)-Pt(1)-Cl(2) | 174.38(5) |
| Pt(1)-Cl(2) | 2.3246(6) | N(2)-Pt(1)-Cl(1) | 174.97(6) |

[a]Numbers in parentheses are estimated standard deviations in the last significant figures. Atoms are labeled as indicated in Figure 2.

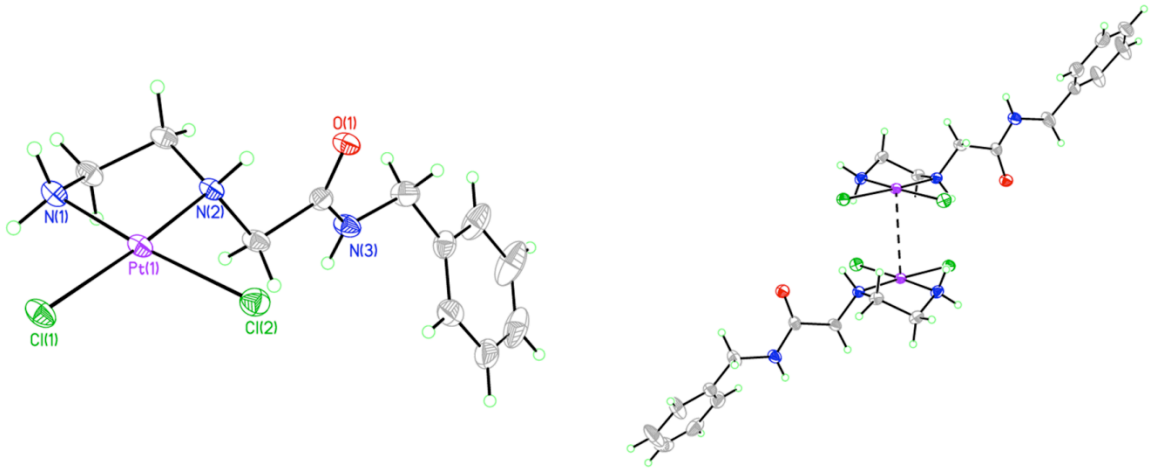


**Fig. 2.** ORTEP diagrams of **1**. The intermolecular Pt-Pt interaction is shown at the right. Ellipsoids are drawn at 50% probability levels.

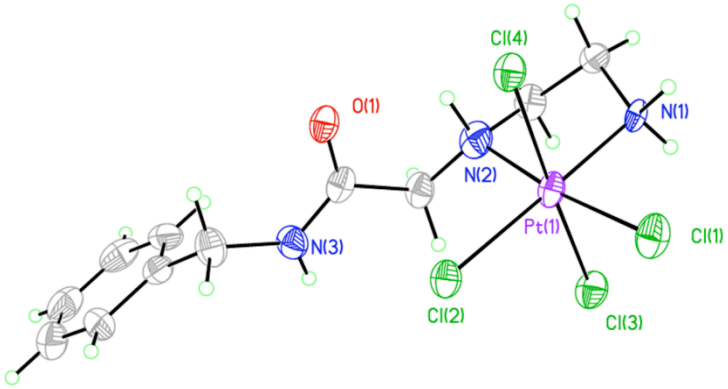


**Fig. 3.** ORTEP diagram of **3**. Ellipsoids are drawn at the 50% probability level.

**Table 3.** Selected Interatomic Distances (Å) and Angles (deg) for **3**.[a]

| Bonds | | Angles | | | | | |
|---|---|---|---|---|---|---|---|
| Pt(1)-N(1) | 2.017(4) | N(1)-Pt(1)-N(2) | 83.30(18) | N(2)-Pt(1)-Cl(2) | 94.22(14) | Cl(3)-Pt(1)-Cl(2) | 90.09(5) |
| Pt(1)-N(2) | 2.109(6) | N(1)-Pt(1)-Cl(1) | 91.12(12) | N(2)-Pt(1)-Cl(3) | 91.87(14) | Cl(4)-Pt(1)-Cl(2) | 93.27(5) |
| Pt(1)-Cl(1) | 2.3041(15) | N(1)-Pt(1)-Cl(2) | 177.20(12) | N(2)-Pt(1)-Cl(4) | 85.70(14) | Cl(3)-Pt(1)-Cl(4) | 175.99(5) |
| Pt(1)-Cl(2) | 2.3216(14) | N(1)-Pt(1)-Cl(3) | 88.69(13) | Cl(1)-Pt(1)-Cl(2) | 91.43(5) | | |
| Pt(1)-Cl(3) | 2.3065(14) | N(1)-Pt(1)-Cl(4) | 87.86(13) | Cl(1)-Pt(1)-Cl(3) | 91.06(6) | | |
| Pt(1)-Cl(4) | 2.3189(14) | N(2)-Pt(1)-Cl(1) | 173.63(15) | Cl(1)-Pt(1)-Cl(4) | 91.05(5) | | |

[a]Numbers in parentheses are estimated standard deviations in the last significant figures. Atoms are labeled as indicated in Figure 3.

The structure of **3** is shown in Figure 3, and relevant bond distances and angles are reported in Table 3. As observed in the crystal structure of **1**, a molecule of DMF is present and forms a hydrogen bond with the proton of the amide group ($O_{DMF}\cdots N_{amide}$ = 2.81 Å). The coordination geometry of **3** is octahedral, as expected for a platinum(IV) complex. The Pt–Cl bond distances are close to 2.3 Å at both the axial and the equatorial sites.

*3.2. Electrochemistry*

The cyclic voltammograms of the two platinum(IV) complexes, **3** and **4**, were recorded in DMF with 0.1 M $Bu_4N(PF_6)$ as the supporting electrolyte (Figure 4). The cathodic peak potentials measured at a scan rate of 100 mV/s for **3** and **4** are at approximately –0.3 V versus Ag/AgCl. For the analogous compound, *cis*-$[Pt(NH_3)_2Cl_4]$, the measured peak potential under identical conditions is –0.45 V [44]. This result indicates that **3** and **4** are easier to reduce than *cis*-$[Pt(NH_3)_2Cl_4]$, despite similar $N_2Cl_4$ coordination sphere. The presence of electron-withdrawing amide groups in **3** and **4** may produce this positive shift in the peak potential and facilitate their reduction.

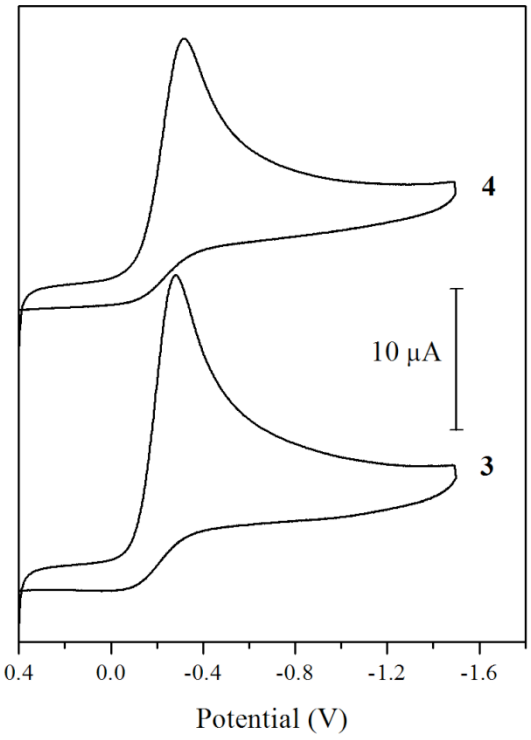


**Fig. 4.** Cyclic voltammograms of **3** (bottom) and **4** (top) measured at a scan rate of 100 mV/s in DMF with 0.1 M $(Bu_4N)(PF_6)$ as the supporting electrolyte. The potential is reported vs Ag/AgCl.

*3.3. Photophysical Properties*

The absorption and emission properties of the fluorescent compounds **2**, **4**, and Ds-en were measured in both DMF and phosphate-buffered saline (PBS) at pH = 7.4. The results are summarized in Table 4. In DMF, the absorption and emission maxima of the three compounds are nearly identical. This result is expected because the optical properties of both compounds are dominated by relatively intense π-π* transitions of the dansyl fluorophore. In moving from DMF to water, the absorption maxima of the three compounds are blue-shifted by 10 nm, and the emission maxima are red-shifted by approximately 40 nm. As seen in Table 4, the emission

quantum yields depend on both the presence of the platinum center and its oxidation state, as well as the solvent. In DMF, the platinum(II) center of **2** slightly quenches the emission, with the quantum yield dropping to 27% from the 40% value measured for free Ds-en. The relatively high quantum yield of 27% is in contrast to prior results from our laboratory in which the presence of a platinum(II) center lowered the quantum yield of a dansylated ligand by a factor of 15 [45]. In the previous system, however, the dansyl fluorophore was positioned much more closely to the platinum(II) center. Quenching of dansyl fluorescence by platinum(II) through the heavy-atom effect thus depends on the spatial separation between the two moieties [46]. The higher quantum yield of **2** most likely derives from the long distance of the dansyl fluorophore from the platinum(II) center. The emission quantum yield of the platinum(IV) complex, **4**, in DMF is only 1.6%, significantly less than that of **2**. This result indicates **4** to be a good candidate for displaying the desired fluorescence turn-on response upon reduction to Pt(II).

**Table 4.** Photophysical Properties of **2** and **4** in DMF and Buffered Aqueous Solution.[a]

| compound | absorption in DMF | absorption in PBS | emission in DMF | emission in PBS |
|---|---|---|---|---|
| | $\lambda_{max}$ (nm), $\varepsilon \times 10^3$( $M^{-1}$•$cm^{-1}$) | $\lambda_{max}$ (nm), $\varepsilon \times 10^3$ ($M^{-1}$•$cm^{-1}$) | $\lambda_{em}$ (nm), $\Phi$ | $\lambda_{em}$ (nm), $\Phi$ |
| **2** | 339, 4.8(2) | 328, 4.6(1) | 520, 0.27(1) | 560, 0.033(2) |
| **4** | 333, 5.19(8) | 325, 5.1(1) | 520, 0.016(1) | 560, 0.0027(9) |
| **Ds-en** | 339, 4.7(1) | 328, 4.6(1) | 520, 0.40(2) | 555, 0.032(3) |

[a]Numbers in parentheses are the standard deviations in the last significant figures derived from at least three independent measurements

In moving from DMF to PBS, significant fluorescence quenching occurs for all three compounds. The quantum yields of Ds-en and **2** drop to values of 3.2 and 3.3%, respectively. This result is expected because the emission of the dansyl fluorophore depends strongly on

solvent polarity [47]. Importantly, the increased quenching effect of the platinum(IV) compound, **4**, carries over to the aqueous environment where the 0.27% quantum yield for emission is still much lower than that of **2**. In water, **4** will therefore elicit a fluorescence turn-on response when reduced to platinum(II), as described below.

*3.4. DFT Calculations*

Time-dependent DFT (TDDFT) calculations were performed to gain an understanding of the origin of the decreased emission of **4** relative to that of **2**. The frontier molecular orbital diagrams of **2** and **4** are shown in Figure 5. The HOMO for both complexes is a dansyl-based π orbital. The LUMOs of **2** and **4** are different, however. In the case of **2**, the LUMO, like the HOMO, is a dansyl-based π orbital. In **4**, the octahedral coordination geometry shifts the energies of the $d_{x2-y2}$ and $d_{z2}$ metal orbitals to an energy that lies between those of the dansyl-based occupied and unoccupied orbitals, resulting in a LUMO that is metal-based. To understand how these molecular orbitals affect the photophysical properties of the complexes, the 50 lowest energy singlet excited states were computed for both **2** and **4** (Tables S3 and S4, Supplementary Data). Both compounds are computed to have an identical, dansyl-based excited state in the visible region (3.32 eV, 373 nm) with a large oscillator strength ($f = 0.1741$), corresponding to the HOMO–LUMO transition for **2** and the HOMO–LUMO+2 transition for **4** (Fig. 5). This excited state transition is the only one that is strongly allowed following irradiation with visible light ($\lambda > 310$ nm, $f > 0.01$), and it is therefore responsible for emission as it relaxes to the ground state. If lower energy excited states are available, however, relaxation can occur non-radiatively through them. In **2** only two excited states, both ligand field (d–d) in character, are lower in energy than the allowed HOMO–LUMO transition. Compound **4**, on the other hand, has 15 excited states that are lower in energy than its allowed HOMO–LUMO+2

transition. Of these 15, the first and second lowest energy excited states can be described as π (dansyl) → σ* (platinum) charge-separated states. As shown on the right side of Fig. 5 by the black downward arrows, these excited states provide plausible non-radiative decay pathways that can be rationalized based on molecular orbital energies alone. These competing non-radiative pathways lower the overall quantum yield for emission of **4**, relative to that of **2**.

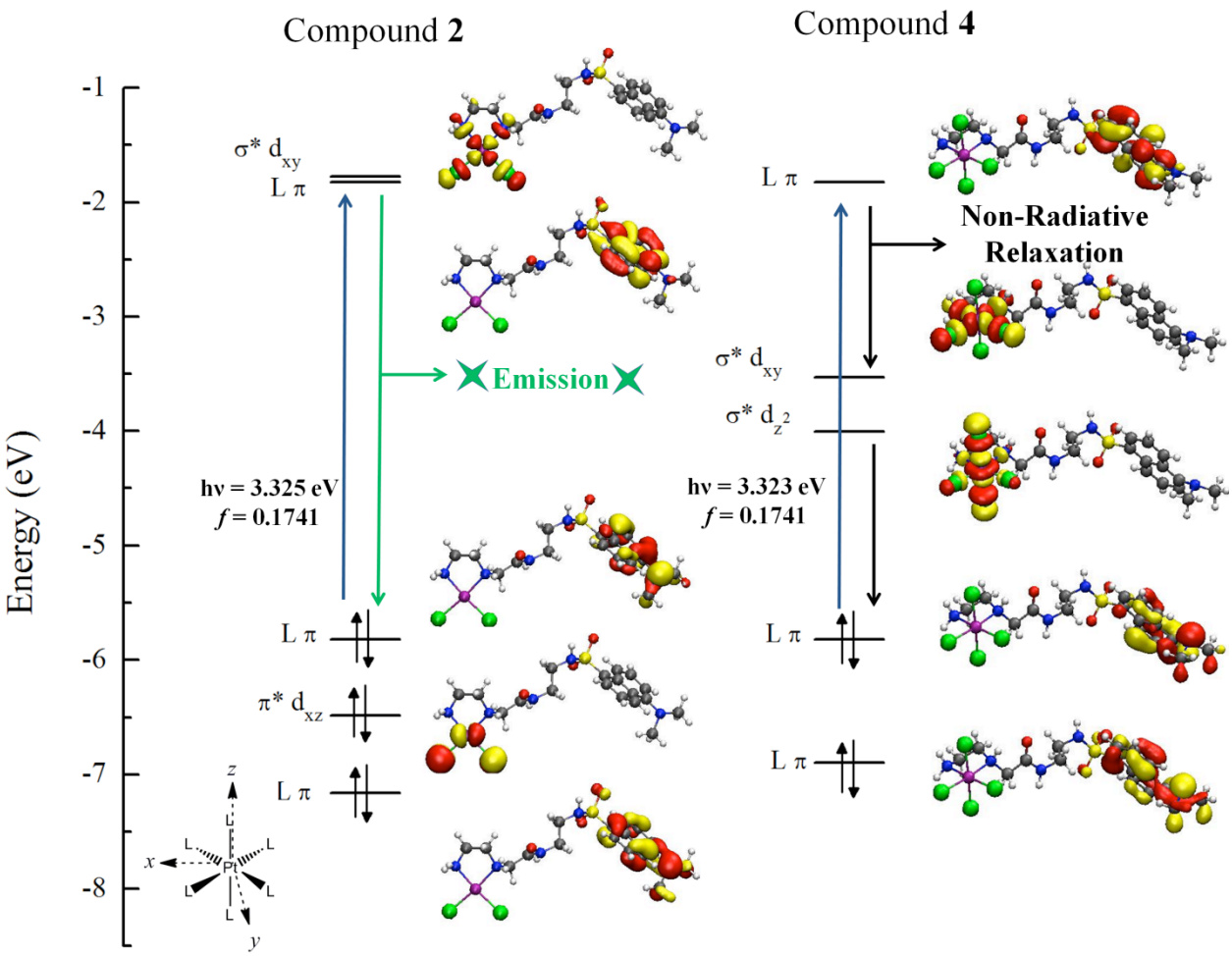


**Fig. 5.** Frontier Kohn-Sham molecular orbital diagram for **2** (left) and **4** (right).

*3.5. Response to Reducing Agents*

Figure 6 displays the emission turn-on response induced by treatment of **4** with a 10-fold excess of glutathione in PBS at pH 7.4. Substitution of other biological reducing agents, cysteine and ascorbic acid, for glutathione afforded nearly identical results. The magnitude and speed of the turn-on response is the same for the three reducing agents. Within a minute after addition of the reducing agents, the turn-on response is complete, with no further increase in emission for up to 15 minutes. The kinetic behavior of this turn-on response is consistent with the ability of ascorbic acid to rapidly reduce a similar compound, $[Pt(en)Cl_4]$ [48].

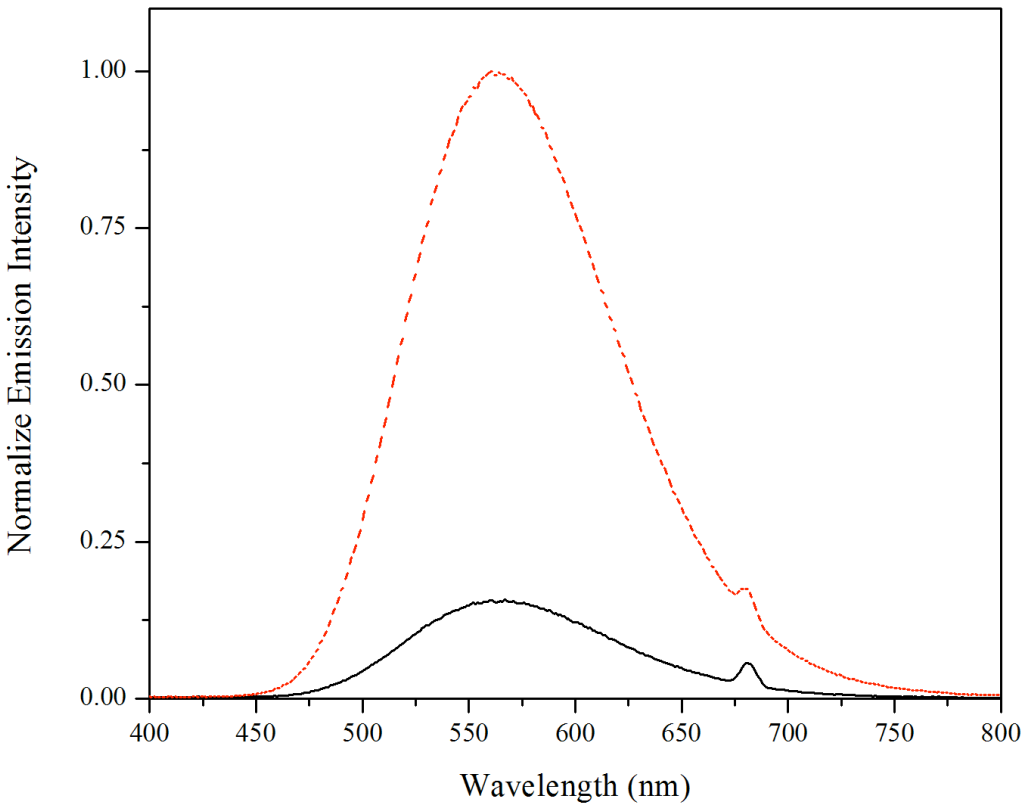


**Fig. 6.** Emission spectra of **4** before (black line) and after addition of 10-fold excess of glutathione (red dashes) in pH 7.4 phosphate-buffered saline. The small peak at 680 nm arises from scattered excitation light ($\lambda_{ex}$ = 340 nm).

The turn-on response upon reduction affords a 6.3-fold increase in integrated emission intensity. Control experiments were carried out in which **4** was treated with the non-reducing amino acid glycine, and the platinum(II) complex, **2**, was similarly treated with glycine as well as the three biological reducing agents. The emission of **2** did not change upon introduction of any of the four compounds, as anticipated. When **4** was treated with glycine, a 1.2-fold increase in emission was observed after several scans and minutes. In an additional control experiment, **4**

alone in buffer showed a similar emission increase after several scans in the fluorimeter. This small but noticeable emission increase most likely arises from photoreduction of **4** in the fluorimeter. Such photoreduction of the metal center is consistent with the proposed fluorescence quenching mechanism by which non-radiative relaxation occurs through the population of metal-based orbitals.

**4. Summary and Conclusions**

Dansyl-bearing fluorescent platinum(II) and platinum(IV) complexes have been synthesized together with non-fluorescent analogues. The non-fluorescent analogues have been crystallographically characterized. The synthetic methodology employed for the syntheses of **1** and **2** has sufficient generality to facilitate the preparation of platinum(II) complexes bearing a variety of peripheral functional groups. The simple amide-coupling chemistry employed should aid in the development of novel platinum(II) complexes for anticancer screening. The results of our photophysical studies demonstrate selective fluorescence quenching in the platinum(IV), compound **4**, compared to the platinum(II), **2**, state. TDDFT calculations indicate that the quenching arises from the presence of metal-based d orbitals energetically positioned between the HOMO and LUMO of the dansyl fluorophore. Addition of reducing agents to **4** triggers a 6.3-fold emission turn-on response in aqueous buffer. Compound **4** therefore has the potential to serve as a mechanistic probe to monitor the reduction platinum(IV) complexes in biology. In theory, such a turn-on response should enable both spatial and temporal resolution of the platinum(IV) reduction event by fluorescence microscopy. Unfortunately, the practical applicability of this complex in living cells is limited by its low quantum yield in water and the rapid rate of reduction. As a first generation platinum(IV) redox sensor, however, compound **4**

provides a proof of concept and starting point for the design of more effective sensors of the properties of platinum(IV) complexes in biological milieu.

**Acknowledgements**

This work was supported by Grant CA034992 from the National Cancer Institute. Spectroscopic instrumentation at the MIT DCIF is maintained with funding from NIH Grant 1S10RR13886-01.

**Appendix A. Supplementary material**

CCDC 848963 and 848964 contain the supplementary crystal data for **1**·DMF and **3**·DMF, respectively. These data can be obtained free of charge from the Cambridge Crystallographic Data Centre via www.ccdc.cam.ac.uk/data_request/cif. Supplementary data associated with this article can be found, in the online version, at doi:xxxxxxxxx.

**References:**

[1] Y. Jung, S.J. Lippard, Chem. Rev. 107 (2007) 1387-1407.
[2] L. Kelland, Nat. Rev. Cancer 7 (2007) 573-584.
[3] K.S. Lovejoy, S.J. Lippard, Dalton Trans. (2009) 10651-10659.
[4] B.W. Harper, A.M. Krause-Heuer, M.P. Grant, M. Manohar, K.B. Garbutcheon-Singh, J.R. Aldrich-Wright, Chem. Eur. J. 16 (2010) 7064-7077.
[5] M.D. Hall, T.W. Hambley, Coord. Chem. Rev. 232 (2002) 49-67.
[6] M.D. Hall, R.C. Dolman, T.W. Hambley, Met. Ions Biol. Syst. 42 (2004) 297-322.
[7] M.D. Hall, H.R. Mellor, R. Callaghan, T.W. Hambley, J. Med. Chem. 50 (2007) 3403-3411.
[8] R.C. Dolman, G.B. Deacon, T.W. Hambley, J. Inorg. Biochem. 88 (2002) 260-267.
[9] M.D. Hall, G.J. Foran, M. Zhang, P.J. Beale, T.W. Hambley, J. Am. Chem. Soc. 125 (2003) 7524-7525.
[10] M.D. Hall, C.T. Dillon, M. Zhang, P. Beale, Z. Cai, B. Lai, A.P.J. Stampfl, T.W. Hambley, J. Biol. Inorg. Chem. 8 (2003) 726-732.
[11] R.A. Alderden, H.R. Mellor, S. Modok, M.D. Hall, S.R. Sutton, M.G. Newville, R. Callaghan, T.W. Hambley, J. Am. Chem. Soc. 129 (2007) 13400-13401.
[12] L.D. Lavis, R.T. Raines, ACS Chem. Biol. 3 (2008) 142-155.
[13] C. Molenaar, J.M. Teuben, R.J. Heetebrij, H.J. Tanke, J. Reedijk, J. Biol. Inorg. Chem. 5 (2000) 655-665.
[14] G.V. Kalayda, G. Zhang, T. Abraham, H.J. Tanke, J. Reedijk, J. Med. Chem. 48 (2005) 5191-5202.
[15] R. Safaei, K. Katano, B.J. Larson, G. Samimi, A.K. Holzer, W. Naerdemann, M. Tomioka, M. Goodman, S.B. Howell, Clin. Cancer Res. 11 (2005) 756-767.
[16] R. Bergonzi, L. Fabbrizzi, M. Licchelli, C. Mangano, Coord. Chem. Rev. 170 (1998) 31-46.
[17] L. Fabbrizzi, M. Licchelli, P. Pallavicini, Acc. Chem. Res. 32 (1999) 846-853.
[18] E.J. New, R. Duan, J.Z. Zhang, T.W. Hambley, Dalton Trans. (2009) 3092-3101.
[19] K.B. Nolan, A.A. Soudi, J. Chem. Res. (M) (1978) 1781-1790.

[20] W. Sun, H. Bandmann, T. Schrader, Chem. Eur. J. 13 (2007) 7701-7707.
[21] X.-F. Zhao, C. Zhang, Synthesis 2007 (2007) 551-557.
[22] J.W. Eastman, Photochem. Photobiol. 6 (1967) 55-72.
[23] M.J. Frisch, G.W. Trucks, H.B. Schlegel, G.E. Scuseria, M.A. Robb, J.R. Cheeseman, J. J. A. Montgomery, T. Vreven, K.N. Kudin, J.C. Burant, J.M. Millam, S.S. Iyengar, J. Tomasi, V. Barone, B. Mennucci, M. Cossi, G. Scalmani, N. Rega, G.A. Petersson, H. Nakatsuji, M. Hada, M. Ehara, K. Toyota, R. Fukuda, J. Hasegawa, M. Ishida, T. Nakajima, Y. Honda, O. Kitao, H. Nakai, M. Klene, X. Li, J.E. Knox, H.P. Hratchian, J.B. Cross, V. Bakken, C. Adamo, J. Jaramillo, R. Gomperts, R.E. Stratmann, O. Yazyev, A.J. Austin, R. Cammi, C. Pomelli, J.W. Ochterski, P.Y. Ayala, K. Morokuma, G.A. Voth, P. Salvador, J.J. Dannenberg, V. G. Zakrzewski, S. Dapprich, A.D. Daniels, M.C. Strain, O. Farkas, D.K. Malick, A.D. Rabuck, K. Raghavachari, J.B. Foresman, J.V. Ortiz, Q. Cui, A.G. Baboul, S. Clifford, J. Cioslowski, B.B. Stefanov, G. Liu, A. Liashenko, P. Piskorz, I. Komaromi, R.L. Martin, D.J. Fox, T. Keith, M.A. Al-Laham, C.Y. Peng, A. Nanayakkara, M. Challacombe, P.M.W. Gill, B. Johnson, W. Chen, M.W. Wong, C. Gonzalez, J.A. Pople, Gaussian 03, Gaussian, Inc., Wallingford, CT, 2004.
[24] C. Lee, W. Yang, R.G. Parr, Phys. Rev. B 37 (1988) 785-789.
[25] A.D. Becke, J. Chem. Phys. 98 (1993) 5648-5652.
[26] P.J. Hay, W.R. Wadt, J. Chem. Phys. 82 (1985) 299-310.
[27] W.J. Hehre, R. Ditchfield, J.A. Pople, J. Chem. Phys. 56 (1972) 2257-2261.
[28] M. Cossi, N. Rega, G. Scalmani, V. Barone, J. Comput. Chem. 24 (2003) 669-681.
[29] APEX2, Bruker AXS, Inc., Madison, WI, 2008.
[30] G.M. Sheldrick, SADABS: Area-Detector Absorption Correction, University of Göttingen, Göttingen, Germany, 2008.
[31] G.M. Sheldrick, SHELXTL-97, University of Göttingen, Göttingen, Germany, 2000.
[32] G.M. Sheldrick, Acta Crystallogr. Sect. A 64 (2008) 112-122.
[33] A.L. Spek, PLATON, A Multipurpose Crystallographic Tool, Utrecht University, Utrecht, The Netherlands, 2008.
[34] K.R. Barnes, A. Kutikov, S.J. Lippard, Chem. Biol. 11 (2004) 557-564.
[35] M. Reithofer, M. Galanski, A. Roller, B.K. Keppler, Eur. J. Inorg. Chem. (2006) 2612-2617.
[36] G.N. Kaluđerović, H. Schmidt, S. Schwieger, C. Wagner, R. Paschke, A. Dietrich, T. Mueller, D. Steinborn, Inorg. Chim. Acta 361 (2008) 1395-1404.
[37] M.S. Robillard, A.R.P.M. Valentijn, N.J. Meeuwenoord, G.A. van der Marel, J.H. van Boom, J. Reedijk, Angew. Chem., Int. Ed. 39 (2000) 3096-3099.
[38] M.S. Robillard, M. Bacac, H. van den Elst, A. Flamigni, G.A. van der Marel, J.H. van Boom, J. Reedijk, J. Comb. Chem. 5 (2003) 821-825.
[39] S.J. Berners-Price, L. Ronconi, P.J. Sadler, Prog. Nucl. Magn. Reson. Spectrosc. 49 (2006) 65-98.
[40] P.S. Pregosin, Coord. Chem. Rev. 44 (1982) 247-291.
[41] B.M. Still, P.G.A. Kumar, J.R. Aldrich-Wright, W.S. Price, Chem. Soc. Rev. 36 (2007) 665-686.
[42] J. Iball, M. MacDougall, S. Scrimgeour, Acta Crystallogr. Sect. B. 31 (1975) 1672-1674.
[43] L.T. Ellis, T.W. Hambley, Acta Crystallogr. Sect. C 50 (1994) 1888-1889.
[44] J.J. Wilson, S.J. Lippard, Inorg. Chem. 50 (2011) 3103-3115.
[45] J.J. Wilson, J.F. Lopes, S.J. Lippard, Inorg. Chem. 49 (2010) 5303-5315.
[46] A.M. Christoforou, P.A. Marzilli, L.G. Marzilli, Inorg. Chem. 45 (2006) 6771-6781.
[47] Y.-H. Li, L.-M. Chan, L. Tyer, R.T. Moody, C.M. Himel, D.M. Hercules, J. Am. Chem. Soc. 97 (1975) 3118-3126.
[48] S. Choi, C. Filotto, M. Bisanzo, S. Delaney, D. Lagasee, J.L. Whitworth, A. Jusko, C. Li, N.A. Wood, J. Willingham, A. Schwenker, K. Spaulding, Inorg. Chem. 37 (1998) 2500-2504.

**Graphical Abstract:**